

Behavior of RC beams under impact loading: some new findings

S.M. Soleimani

Associated Engineering Ltd., Burnaby, BC, Canada

N. Banthia & S. Mindess

The University of British Columbia, Vancouver, BC, Canada

ABSTRACT: The load recorded by the striking tup has been used to study the impact behavior of reinforced concrete beams. It was noted that this load could not be considered as the bending load experienced by the concrete beam. A portion of this load is used to accelerate the beam, and therefore, finding the exact bending load versus time response has been one of the most challenging tasks for impact researchers. To capture a true bending load versus time response a special test setup was designed and built. Tests showed a time lag between the maximum load indicated by the instrumented tup and the maximum load indicated by the instrumented supports. This time lag has confirmed that the inertial load effect must be taken into account. It was also found that beyond a certain impact velocity, the flexural load capacity of RC beams remained constant; further increases in stress rate did not increase their load carrying capacity.

1 INTRODUCTION

Material properties change under high strain rates. As a result, reinforced concrete (RC) beams made of reinforcing bars and concrete will respond differently at different loading rates. Since the compressive (and tensile) strength of concrete and the yield strength of steel increase when loaded at high strain rates, increasing the strain rate will generally increase the flexural capacity of RC beams (Takeda and Tachikawa 1971, Bertero et al. 1973, Kishi et al. 2001).

2 IMPACT TEST SETUP

2.1 Drop weight impact machine

A drop weight impact machine with a capacity of 14.5 kJ was used in this research study. A mass of 591 kg (including the striking tup) can be dropped from as high as 2.5 m. During a test, the hammer is raised to a certain height above the specimen using a hoist and chain system. At this position, air brakes are applied on the steel guide rails to release the chain from the hammer. On releasing the brakes, the hammer falls and strikes the specimen. Three load cells were designed and built at the University of British Columbia for this project. During preliminary tests, it was discovered that if the specimen was not prevented from vertical movements at the supports, within a very short period after first contact of the hammer with the specimen, contact with the

supports was lost and as a result, loads indicated by the support load cells were not correct. For instance, the loads recorded by the support load cells for two identical tests were totally different. This phenomenon was further verified by using a high speed camera. To overcome this problem, the vertical movement of RC beams at the supports was restrained using two steel yokes (Figure 1). In order to assure that the beams were still simply supported, these yokes were pinned at the bottom to allow rotation during beam loading. To permit an easier rotation, a round steel bar was welded underneath the top steel plate where the yoke touched the beam.



Figure 1. Impact test setup with steel yokes.

2.2 Beam design and testing procedure

A total of 12 identical RC beams were cast to investigate the behavior of RC beams under impact loading. These beams contained flexural as well as shear reinforcement. They were 1 m in total length and were tested over an 800 mm span. Load configuration and cross-sectional details are shown in Figure 2.

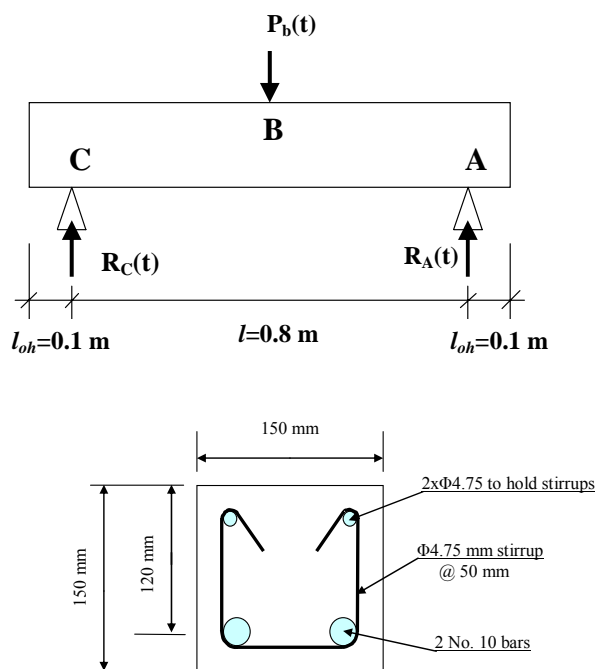


Figure 2. Load configuration and cross-sectional details of RC beams.

Seven beams were tested under impact with different impact velocities ranging from 2.8 m/s to 6.26 m/s, and three beams were tested under quasi-static, 3-point loading. The remaining two beams were strengthened by GFRP fabric; one was tested under quasi-static and the other under impact loading (impact velocity = 3.43 m/s). Table 1 shows the beam designations and configuration.

Based on the Canadian Concrete Design Code, the capacity of this beam under quasi-static loading

is 51 kN, when the tension reinforcement starts to yield. It is worth noting that the beam was designed to fail in a flexural mode, since enough stirrups were provided to prevent shear failure.

Under quasi-static loading conditions, all of the beams (i.e. BS-1, BS-2, BS-3 and BS-FRP) were tested in 3-point loading using a Baldwin 400 kip Universal Testing Machine. Under impact loading conditions, all of the beams were tested using an instrumented drop-weight impact machine as explained in 2.1.

3 RESULTS AND DISCUSSION

3.1 Quasi-static loading

The results of the three beams loaded quasi-statically (i.e. BS-1, BS-2 and BS-3) were quite consistent. The load vs. deflection curve for beam BS-1, shown in Figure 3, represents a typical flexural failure mode of RC beams. Load vs. deflection responses for the other two beams (BS-2 and BS-3) were very similar to that of beam BS-1. Initially, the beam was uncracked (i.e. from the beginning of the curve till Point A). The cross-sectional strains at this stage were very small and the stress distribution was essentially linear. When the stresses at the bottom side of the beam reached the concrete tensile strength, cracking occurred. This is shown as Point A in Figure 3. After cracking, the tensile force in the concrete was transferred to the steel reinforcing bars (rebars). As a result, less of the concrete cross section was effective in resisting moments and the stiffness of the beam (i.e. the slope of the curve) decreased. Eventually, as the applied load increased, the tensile reinforcement reached the yield point shown by Point B in Figure 3. Once yielding had occurred, the mid-span deflection increased rapidly with little increase in load carrying capacity. The beam failed due to crushing of the concrete at the top of the beam. The experimental test result showed 54 kN capacity for this beam, corresponding to Point B in Figure 3. Thus there is a good agreement between theoretical and experimental values for the load carrying capacity of this RC beam.

3.2 Impact loading

For all impact tests using the drop-weight machine, PCB Piezotronics™ accelerometers were employed. These accelerometers were screwed into mounts which were glued to the specimens prior to testing. Vertical accelerations at different locations along the beam were recorded with a frequency of 100 kHz using National Instruments™ VI Logger software. Locations of the accelerometers are shown in Figure 4.

Table 1. RC beams designations.

Beam No.	Quasi-static Loading	Impact Loading Drop Height, h (mm)					GFRP Fabric
		400	500	600	1000	2000	
BS-1	✓	---	---	---	---	---	---
BS-2	✓	---	---	---	---	---	---
BS-3	✓	---	---	---	---	---	---
BS-FRP	✓	---	---	---	---	---	✓
BI-400	---	✓	---	---	---	---	---
BI-500-1	---	---	✓	---	---	---	---
BI-500-2	---	---	✓	---	---	---	---
BI-500-3	---	---	✓	---	---	---	---
BI-600	---	---	---	✓	---	---	---
BI-1000	---	---	---	---	✓	---	---
BI-2000	---	---	---	---	---	✓	---
BI-600-FRP	---	---	---	✓	---	---	✓

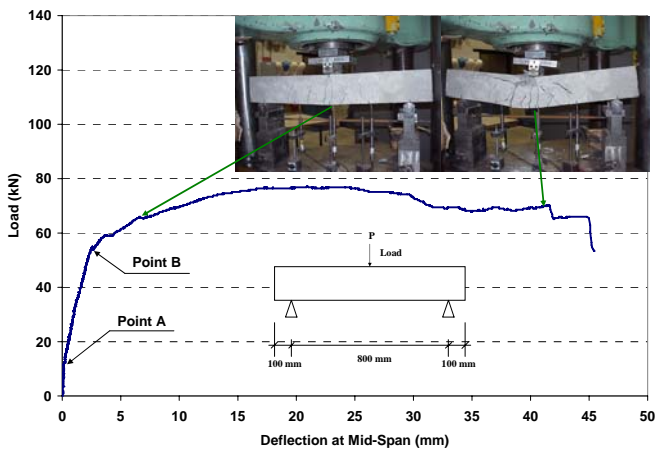


Figure 3. Load vs. deflection curve for RC beam with a flexural failure mode.

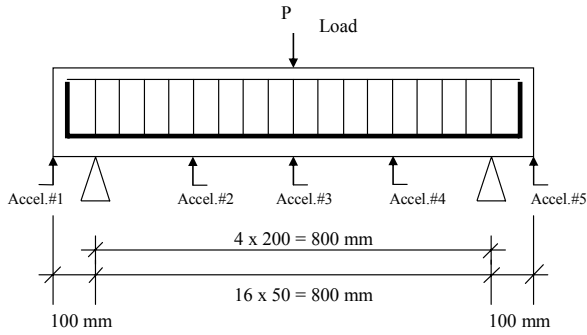


Figure 4. Location of the accelerometers in impact loading.

The velocity and displacement histories at the location of the accelerometers were obtained by integrating the acceleration history with respect to time using the following equations:

$$\dot{u}_0(t) = \int \ddot{u}_0(t) dt \quad (1)$$

$$u_0(t) = \int \dot{u}_0(t) dt \quad (2)$$

where $\ddot{u}_0(t)$ = acceleration at the location of the accelerometer; $\dot{u}_0(t)$ = velocity at the location of the accelerometer; and $u_0(t)$ = displacement at the location of the accelerometer.

The contact load between the specimen and the hammer is not the true bending load on the beam, because of the inertial reaction of the beam. A part of the tup load is used to accelerate the beam from its rest position. D'Alembert's principle of dynamic equilibrium can be used to write equilibrium equations in dynamic load conditions. This principle is based on the notion of a fictitious inertial force. This force is equal to the product of mass times its acceleration and acting in a direction opposite to the acceleration. D'Alembert's principle of dynamic equilibrium states that with inertial forces included, a system is in equilibrium at each time instant. As a result, a free-body diagram of a moving mass can be

drawn and principles of statics can be used to develop the equations of motion. Thus, one can conclude that in order to obtain the actual bending load on the specimen the inertial load must be subtracted from the observed tup load. It is also important to note that the tup load throughout this paper is taken as a point load acting at the mid-span of the beam, whereas the inertial load of the beam is a body force distributed throughout the body of the beam. This distributed body force can be replaced by an equivalent inertial load, which can then be subtracted from the tup load, to obtain the true bending load, which acts at the mid-span. Therefore, at any time t , the following equation can be used to obtain the true bending load that the beam is experiencing (Banthia et al., 1989):

$$P_b(t) = P_t(t) - P_i(t) \quad (3)$$

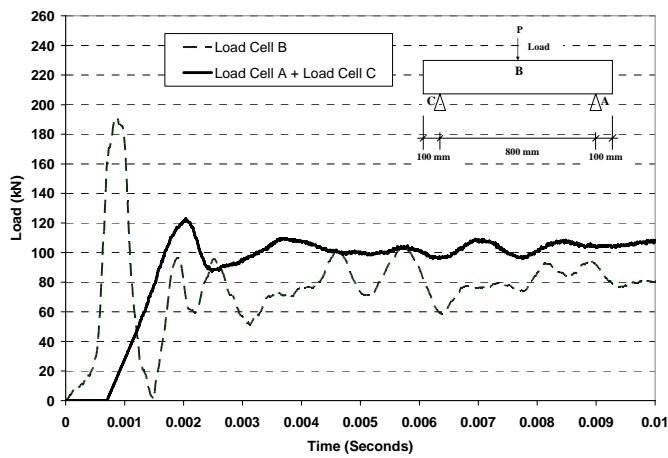
where $P_b(t)$ = true bending load at the mid-span of the beam at time t ; $P_t(t)$ = tup load at time t ; and $P_i(t)$ = point load representing the inertial load at the mid-span of the beam at time t equivalent to the distributed inertial load.

In this research program, support anvils in addition to the tup were instrumented in order to obtain valid and true bending loads at any time t directly from the tests. Therefore, the true bending load at time t , $P_b(t)$, which acts at the mid-span can also be obtained by adding the reaction forces at the support anvils at time t :

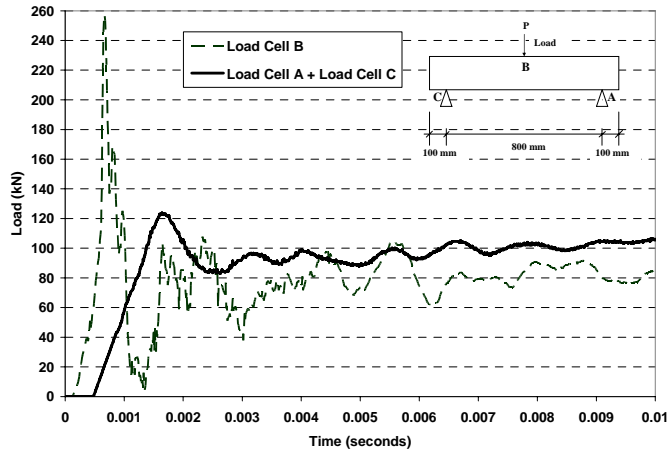
$$P_b(t) = R_A(t) + R_C(t) \quad (4)$$

where $R_A(t)$ = reaction load at support A at time t ; and $R_C(t)$ = reaction load at support C at time t as shown in Figure 2. This has been verified experimentally by Soleimani (2006).

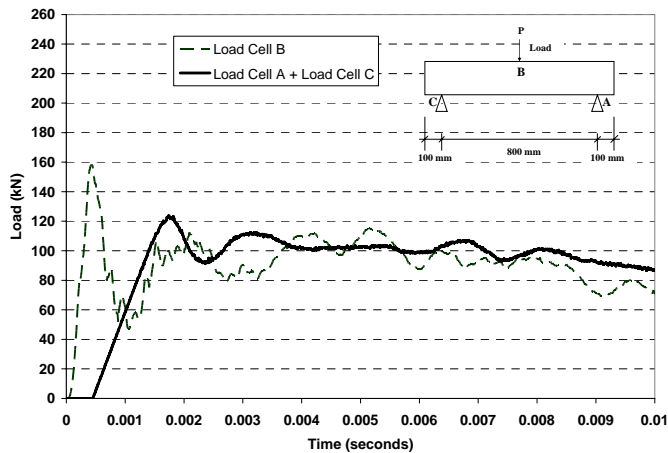
Three identical beams (i.e. BI-500-1, BI-500-2 and BI-500-3) were tested under a 500 mm drop height and steel yokes were used to prevent upward movement of beams at the support locations at the instant of impact. Load vs. time histories of these beams are shown in Figure 5 (a) to (c). There are two important points to mention here: (1) true bending load, $P_b(t)$, obtained from support load cells (load cell A + load cell C) are pretty much the same for all three beams; (2) maximum tup load (denoted as load cell B) recorded by the striking hammer is not consistent and is in the range of 158 kN to 255 kN. It is also worth mentioning that the results obtained from the two support load cells are quite similar to each other and the peak load in both load cells occurred at the same time as expected. This phenomenon can be seen in Figure 6 for the case of beam B1-500-2.



(a)



(b)



(c)

Figure 5. Load vs. time for beam (a) BI-500-1; (b) BI-500-2; and (c) BI-500-3.

Equations 1 and 2 were used to calculate the displacement of the RC beam at the locations of the accelerometers. For beam BI-500-1, the displacement curve along half of the beam's length is shown in Figure 7. Note that the deflection distribution is essentially linear, consistent with many earlier studies on beams with various types of reinforcement (e.g., Banthia 1987; Bentur et al. 1986). Since the beam failed in flexure, the displacement on the other half of the beam was symmetrical to the displacement shown in this Figure. The diamond-shaped points in this Figure show the actual displacement of the

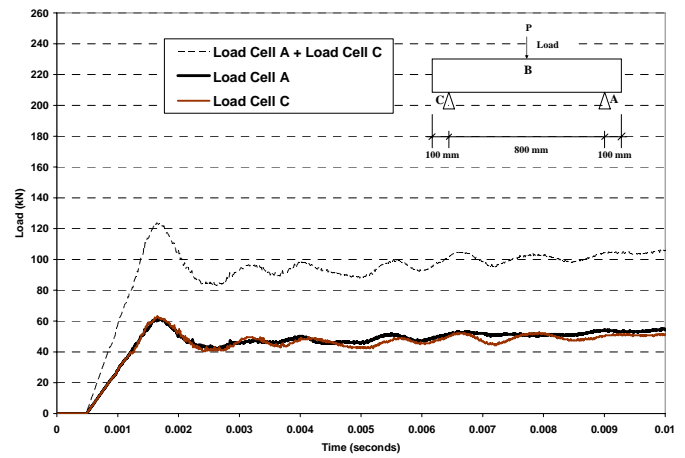


Figure 6. Load vs. time for support load cells in beam BI-500-2.

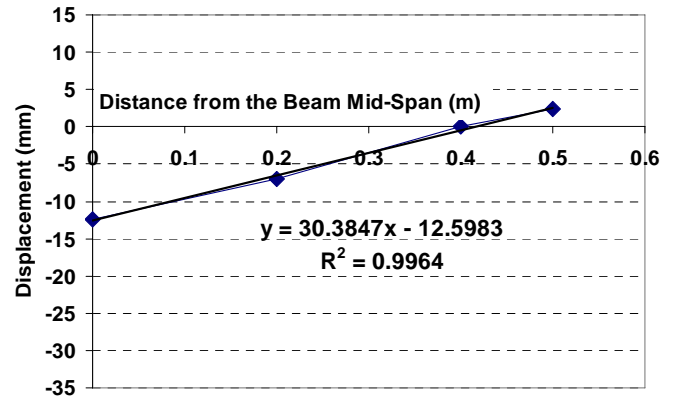


Figure 7. Displacement of beam BI-500-1 at $t = 0.005$ s.

beam. The best-fit line is drawn and its equation along with its R^2 value is given. The displacements shown in Figure 7 were recorded at 0.005 seconds after the impact.

Therefore, one can conclude that the deflected shape for a simply supported RC beam at any time t under impact loading produces a linear deflection profile that can be approximated by a V-shape consisting of two perfectly symmetrical lines.

At the instance of impact, the hammer has a velocity V_h given by:

$$V_h = \sqrt{2gh} \quad (5)$$

where V_h = velocity of the falling hammer at the instance of impact in m/s ; g = acceleration due to gravity ($=9.81 \text{ m/s}^2$); and h = drop height in m.

The impact velocities at the instant of impact for the hammer with a mass of 591 kg for different drop heights, calculated using Equation 5, are given in Table 2.

Table 2. Impact velocity for different drop height.

Drop height (mm)	Velocity (m/s)
400	2.80
500	3.13
600	3.43
1000	4.43
2000	6.26

As an example, the velocity vs. time calculated by Equation 1 for beam BI-500-2 is shown in Figure 8. Interestingly, the velocity of the hammer at the instant of impact (3.13 m/s from Table 2) and the maximum velocity of the beam (which occurred 0.001 s after the impact as shown in Figure 8) are very similar to each other. This, at least to some extent, can explain why the top load at the very beginning of impact decreased almost to zero, after a very rapid increase to a maximum value (see Figure 5). In other words, the beam was accelerated by the hammer and reached its maximum velocity while at the same time (i.e. $t = 0.001$ s) the top load (load cell B) decreased to zero as the beam sped away from the hammer and lost contact. The hammer was back in contact with the beam after some time (in the case of BI-500-2, after about 0.0005 s) and the load rose again. Some time after impact started (in the case of BI-500-2, after 0.035 s) the velocity of both (i.e. hammer and beam) decreased to zero.

The true bending load vs. mid-span deflection curves for beams BI-400, BI-500-1, BI-500-2, BI-500-3, BI-600, BI-1000 and BI-2000 are shown in Figures 9 to 13. The numbers 400, 500, 600, 1000 and 2000 refer to the drop height in mm (see Table 1). Equation 4 was used to find the true bending load and Equations 1 and 2 were used to find the deflection at mid-span from the acceleration histories of mid-span accelerometers (accelerometer #3 in Figure 4) in each case. To provide a meaningful comparison, mid-span deflections are shown out to 50 mm in all cases.

Load vs. mid-span deflection of the same beam tested under static loading is also included in each graph to show the differences in beam responses to different loading rates.

Maximum recorded top loads for beams tested under different drop heights are compared in Figure 16. Maximum recorded true bending loads (summation of support load cells) are shown in Figure 17.

It is clear that while the recorded top load in these beams, in general, increased with increasing drop height, at a constant drop height (i.e. 500 mm), the maximum values for top load were not the same. However, beyond a certain drop height, the maximum true bending load (i.e. load cell A + load cell C) did not change with further increases in drop height.

The bending load at failure vs. impact velocity is shown in Figure 18. Bending load at failure is defined as the maximum recorded true bending load for impact loading. This is also the load at which, presumably, the steel rebars in tension start yielding under static loading.

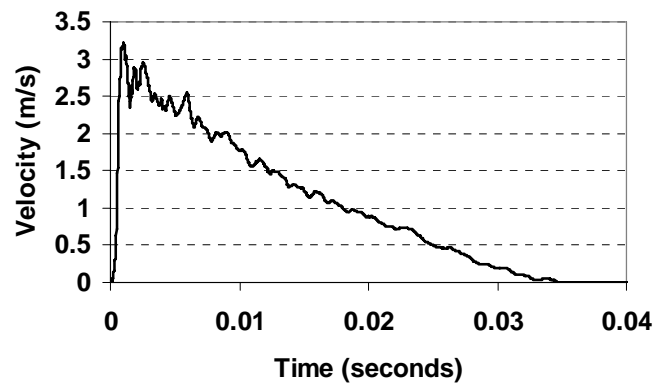


Figure 8. Velocity vs. time at the mid-span, beam BI-500-2.

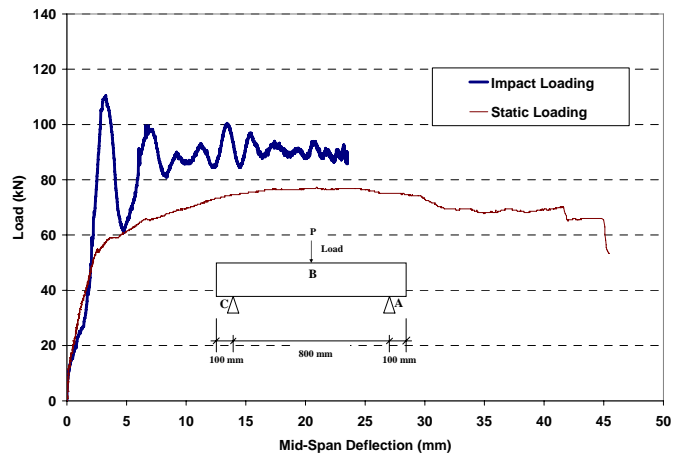


Figure 9. Load vs. mid-span deflection, beam BI-400.

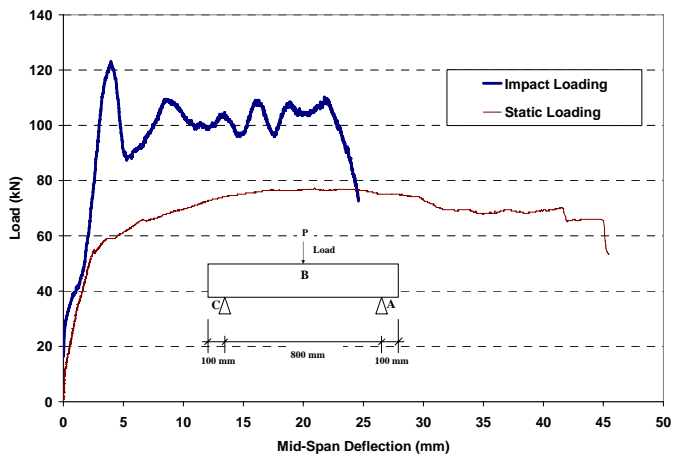


Figure 10. Load vs. mid-span deflection, beam BI-500-1.

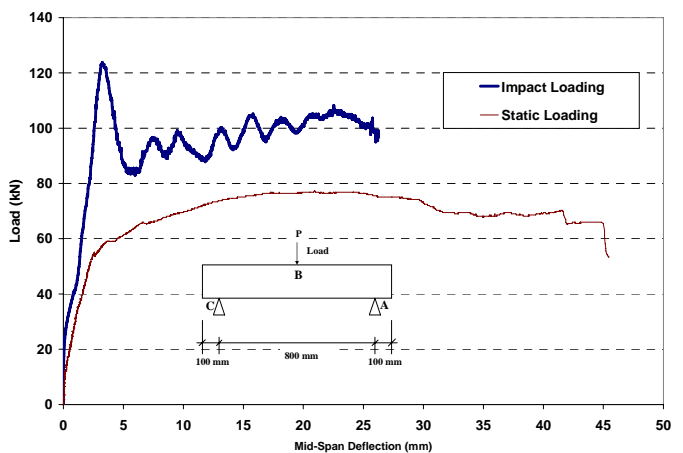


Figure 11. Load vs. mid-span deflection, beam BI-500-2.

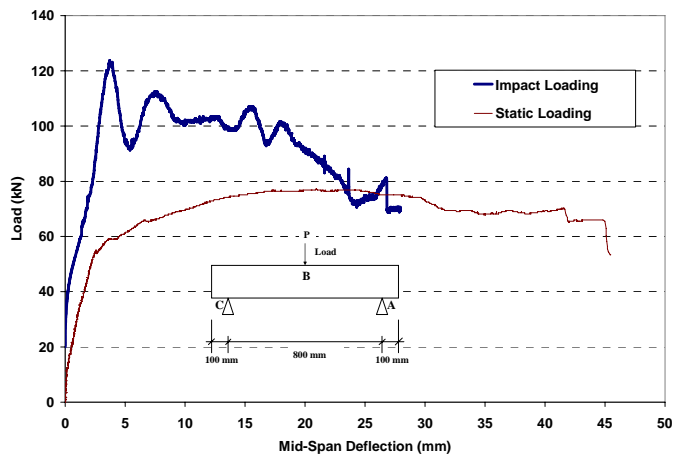


Figure 12. Load vs. mid-span deflection, beam BI-500-3.

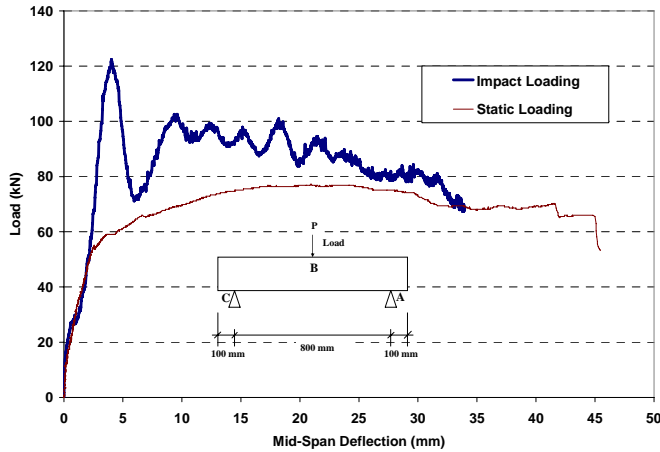


Figure 13. Load vs. mid-span deflection, beam BI-600.

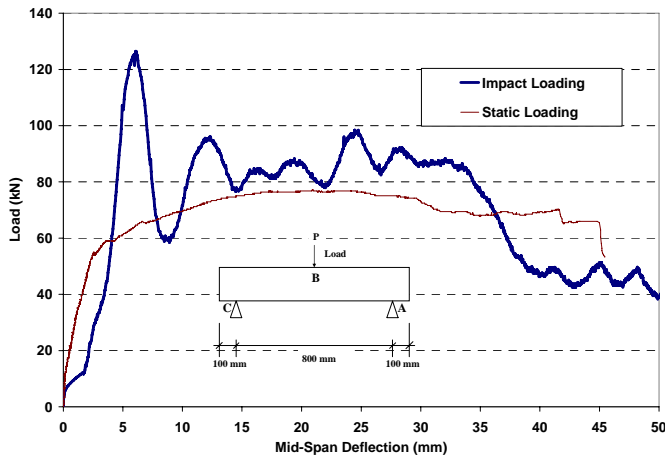


Figure 14. Load vs. mid-span deflection, beam BI-1000.

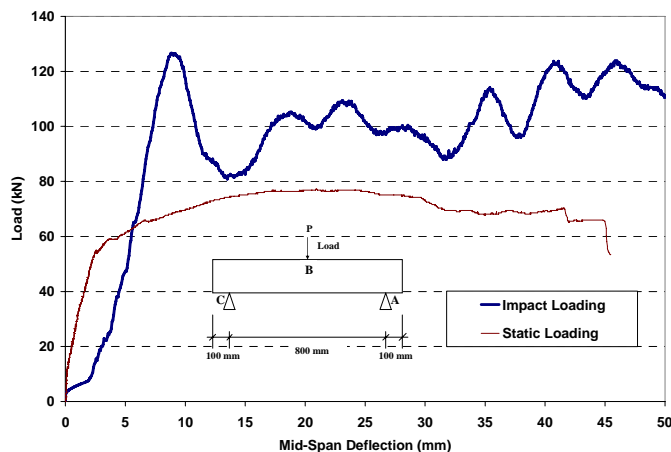


Figure 15. Load vs. mid-span deflection, beam BI-2000.

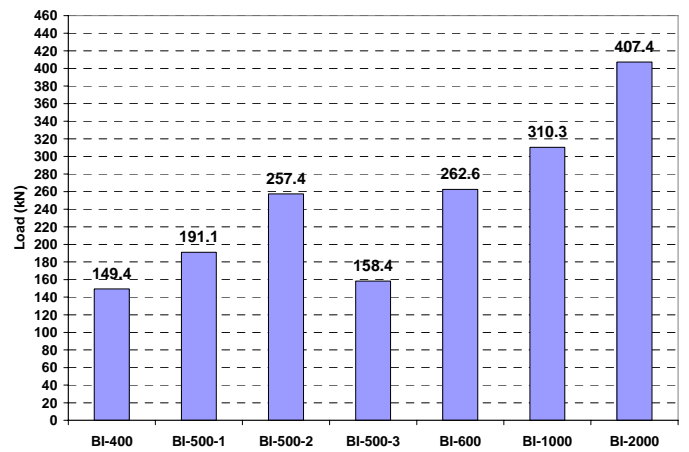


Figure 16. Maximum recorded tup load for different beams/drop height.

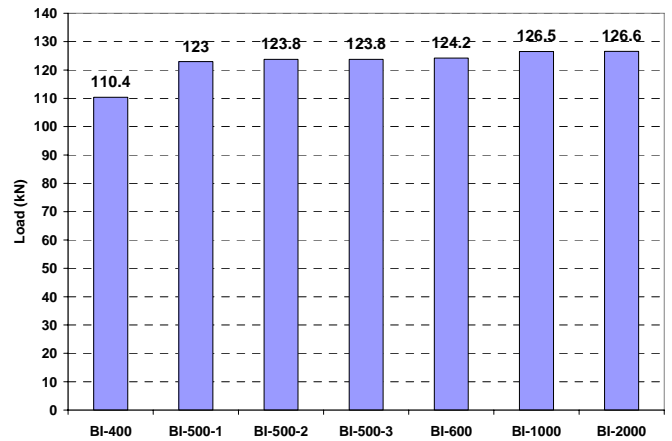


Figure 17. Maximum recorded true bending load for different beams/drop height.

It may be seen that bending load at failure increased with increasing velocity of the impact hammer until it reached a velocity of about 3 m/s. After this point, the bending load at failure was independent of impact velocity and remained constant. It is very important to note that for this hammer, with a mass of 591 kg, a minimum drop height is needed to make the RC beam fail. For example a drop height of only 100 mm of this hammer most probably would not break the beam, but failure might occur if a heavier hammer was employed. Since the impact velocity is directly related to hammer drop height, one can conclude that for a given hammer mass, there exists a certain threshold velocity (or drop height) after which the bending load at failure will not increase with increasing velocity. This threshold velocity for the hammer used in this research was found to be ~ 3 m/s. Figure 18 also shows that the impact bending capacity of this RC beam is about 2.3 times its static bending capacity. Therefore, an impact coefficient of 2.3 can be used to estimate the impact bending capacity of this RC beam from its static bending capacity.

Equation (7.8) can be rewritten as:

$$P_i(t) = P_t(t) - P_b(t) \quad (6)$$

Therefore, the inertial load at any time t is the difference between the tup load and the true bending load. As an example, the inertial load for beam BI-400 calculated by Equation 6 is shown in Figure 19. The values obtained by this equation are the most accurate values coming from a fully instrumented test setup.

A large portion of the peak load measured by the instrumented tup is the inertial load. This is shown in Figure 20. At the peak load measured by the instrumented tup, the inertial load, used to accelerate the beam from its rest position, may account for 75% to 98% of the total load.

3.3 Beams strengthened by GFRP fabric

The Wabo[®] MBrace GFRP fabric system was used to strengthen two RC beams for flexure and shear. One layer of GFRP fabric with a thickness of about 1.2 mm, length of 750 mm and width of 150 mm was applied longitudinally on the tension (bottom) side of the beam for flexural strengthening and an extra layer with fibers perpendicular to the fiber direction of the first layer was applied on 3 sides (i.e. 2 sides and bottom side) for shear strengthening.

One of these beams was tested under quasi-static loading, while the other was tested under impact with a 600 mm hammer drop height (i.e. impact velocity of 3.43 m/s). Load vs. mid-span deflections of these RC beams are shown in Figure 21 (a) and (b). It is important to note that while the control RC beam (i.e. when no GFRP fabric was used) failed in flexure, the strengthened RC beam failed in shear indicating that shear strengthening was not as effective as flexural strengthening; perhaps more layers of GFRP were needed to overcome the deficiency of shear strength in these beams.

In general, these tests showed that GFRP fabric can effectively increase an RC beam's load capacity under both quasi-static and impact load conditions.

Load carrying capacities of these beams are compared in Table 3. While an 84% increase in load carrying capacity was observed in quasi-static loading, the same GFRP system was able to increase the capacity by only 38% under impact loading. It is also worth mentioning that while the maximum bending load under impact loading for the un-strengthened RC beam was 2.26 times its static bending capacity, the ratio of maximum impact load to static load for the strengthened RC beam was only 1.69. This difference can certainly be explained by the change in failure mode from bending to shear when GFRP fabric was applied to these RC beams. The area under the load-deflection curve in Figure 21 (b) was meas-

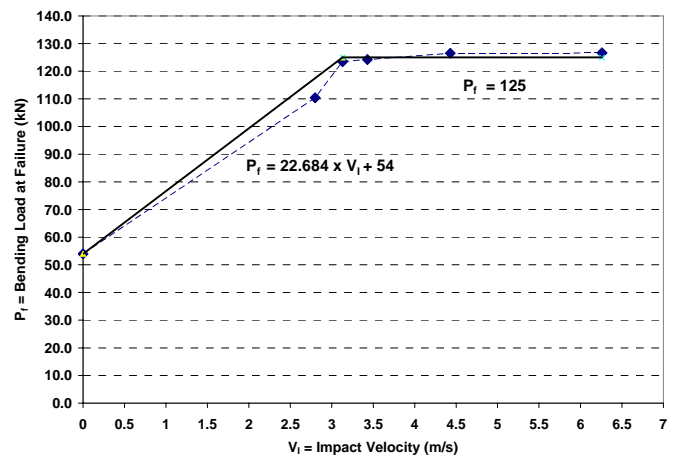


Figure 18. Bending Load at Failure vs. Impact Velocity.

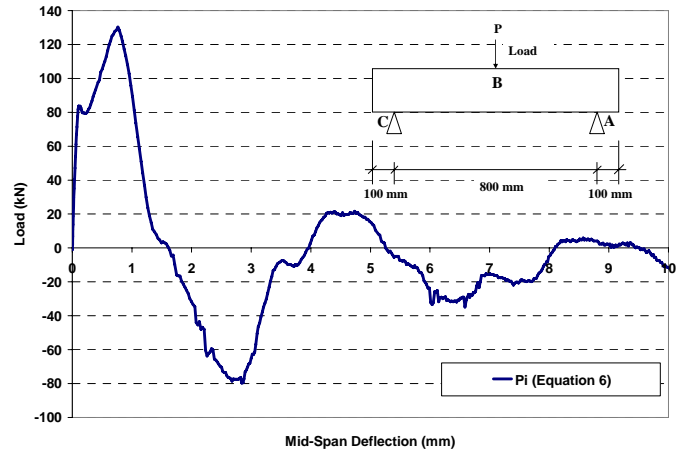


Figure 19. Inertia load for beam BI-400.

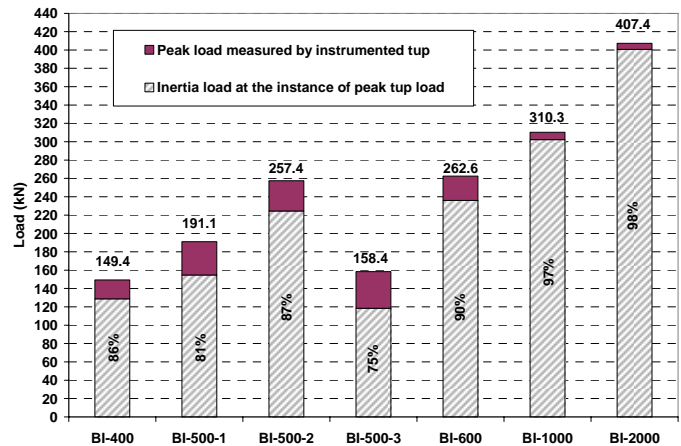


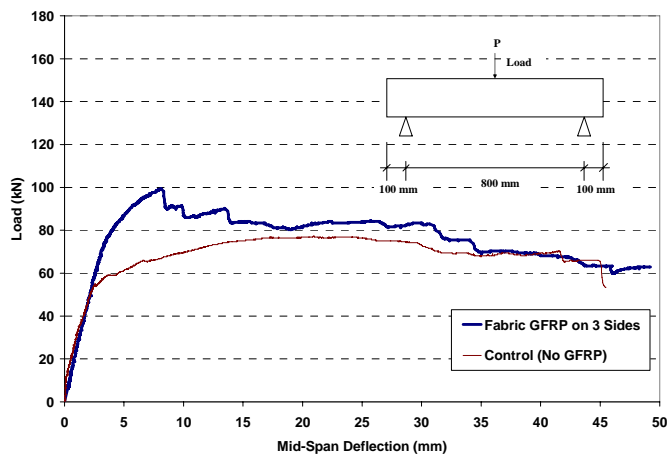
Figure 20. Inertia load at the peak of tup load.

ured and it was found that about 86% of the input energy was absorbed by the strengthened RC beam during the impact.

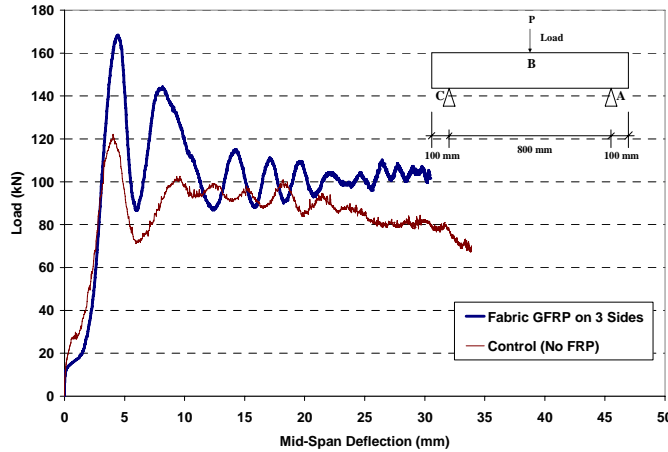
4 CONCLUSIONS

Based on the results and discussions reported above, the following conclusions can be drawn:

1. Load carrying capacity of RC beams under impact loading can be obtained using instrumented anvil supports.



(a)



(b)

Figure 21. Load vs. mid-span deflection for RC beam strengthened in shear and flexure using fabric GFRP; (a) Quasi-static loading, (b) Impact loading (velocity = 3.43 m/s).

Table 3. Load carrying capacity of RC beams strengthened by fabric GFRP.

Loading	Load carrying capacity [kN]	Increase in load carrying capacity [%]
Quasi-static	99.4 (54)*	84%
Impact	168.4 (122.2)*	38%

* Numbers in brackets are the load carrying capacity of un-strengthened RC beams.

2. The use of steel yokes at the support provides more reliable and accurate results.

3. Loads measured by the instrumented tup will result in misleading conclusions due to inertia effect.

4. There is a time lag between the maximum load indicated by the instrumented tup and the maximum load indicated by the instrumented supports. This lag is due to the stress pulse travel time from the centre to the support. This time lag shows that the inertial load effect must be taken into account.

5. Inertial load at any time t can be obtained by subtracting the summation of the support load cells (i.e. true bending load) from the load obtained by the instrumented tup.

6. Bending load capacity of an RC beam under impact loading can be estimated as 2.3 times its

static capacity for the conditions and details of tests performed here. Similar coefficient was reported for different types of RC beams (different cross-sectional areas and different reinforcement ratios) tested under impact loading (Kishi et al. 2001).

7. After a certain impact velocity, the flexural load capacity of RC beams remains constant, and increases in stress (or strain) rate will not increase their load carrying capacity.

8. GFRP fabric can increase the load carrying capacity of RC beams in both static and impact loading conditions.

9. The use of fabric GFRP may change the mode of failure, and as a result, the load carrying capacity of an RC beam strengthened by fabric GFRP under impact loading can be much lower than the anticipated 2.3 times its static capacity (see conclusion 6 above).

REFERENCES

- Banthia, N. 1987. Impact resistance of concrete. PhD Thesis, University of British Columbia, Vancouver, Canada.
- Banthia, N., Mindess, S., Bentur, A. and Pigeon, M. 1989. Impact testing of concrete using a drop-weight impact machine. *Experimental Mechanics* 29(2): 63-69.
- Bentur, A., Mindess, S. and Banthia, N. 1986. The behaviour of concrete under impact loading: experimental procedures and method of analysis. *Materiaux et Constructions*, 19(113): 371-378.
- Bertero, V.V., Rea, D., Mahin, S., and Atalay, M.B. 1973. Rate of loading effects on uncracked and repaired reinforced concrete members. *Proceedings of 5th world conference on earthquake engineering, Rome*. Vol. 1: 1461-1470.
- Kishi, N., Nakano, O., Matsuoka, K.G., and Ando, T. 2001. Experimental study on ultimate strength of flexural-failure-type RC beams under impact loading. *Proceedings of the international conference on structural mechanics in reactor technology*. Washington, DC. Paper # 1525, 7 pages.
- Soleimani, S.M. 2006. Sprayed glass fiber reinforced polymers in shear strengthening and enhancement of impact resistance of reinforced concrete beams. PhD Thesis, University of British Columbia, Vancouver, Canada.
- Takeda, J. and Tachikawa, H. 1971. Deformation and fracture of concrete subjected to dynamic load. *Proceedings of the international conference on mechanical behaviour of materials, Kyoto, Japan*. pp 267-277.